Iranian Journal of Materials Science and Engineering, Vol. 21, Number 3, September 2024
RESEARCH PAPER

On the Magnetic Properties of High Entropy Intermetallic Compounds

Ahmad Ostovari Moghaddam[1,*], Olga Zaitseva[1], Sergey Uporov[2], Rahele Fereidonnejad[1], Dmitry Mikhailov[1], Nataliya Shaburova[1], Evgeny Trofimov[1,*]

* *trofimovea@susu.ru, ostovarim@susu.ru*

[1] South Ural State University, 76 Lenin Av., Chelyabinsk 454080, Russia
[2] Institute of Metallurgy, Ural Branch Russian Academy of Sciences, 101 Amundsen St., Ekaterinburg 620016, Russia

Received: May 2024 **Revised: August 2024** **Accepted: September 2024**
DOI: 10.22068/ijmse.3622

Abstract: *High entropy intermetallic compounds (HEICs) are an interesting class of materials combining the properties of multicomponent solid solutions and the ordered superlattices in a single material. In this work, microstructural and magnetic properties of (CoCuFeMnNi)Al, (CoCuFeMnNi)Zn_3, (FeCoMnNiCr)$_3Sn_2$, (FeCoNiMn)$_3Sn_2$ and Cu_3(InSnSbGaGe) HEICs fabricated by induction melting are studied. The magnetic properties of the HEICs were determined mainly by the nature of the magnetic momentum of the constituent elements. (CoCuFeMnNi)Al and (CoCuFeMnNi)Zn_3 displayed ferromagnetic behavior at 5 K while indicating linear dependency of magnetization vs. magnetic (i.e. paramagnetic or antiferromagnetic state) at 300 K. The magnetization of (FeCoMnNiCr)$_3Sn_2$, (FeCoNiMn)$_3Sn_2$ and Cu_3(InSnSbGaGe) HEICs at 300 K exhibited a nearly linear dependency to magnetic field. Among all the investigated samples, (CoCuFeMnNi)Al exhibited the best magnetic properties with a saturation magnetization of about Ms= 6.5 emu/g and a coercivity of about H_c= 100 Oe.*

Keywords: *High entropy intermetallic compounds, Crystal structure, Magnetic properties.*

1. INTRODUCTION

Recently, high entropy alloys with ordered crystal structures consisting of five or more elements at one sublattice are considered as high entropy intermetallic compounds (HEICs), which typically exhibit interesting mechanical [1, 2], magnetic [3], catalytic [4] and thermal [1, 5] properties. Till now, both transition and refractory elements of the d-block of the periodic table have been mainly used to develop HEICs. This includes Fe, Co, Ni, Mn, Cr and Cu (transition) or Zr, Hf, Nb, Ta, Mo, V, and Ti (refractory) elements, which are used mainly because they exhibit close electronegativity and atomic sizes. However, a combination of transition and refractory elements may be also employed [6]. More recently, structurally ordered PtRhFeNiCu [7] consisting of noble elements, and Cu_3(InSnSbGe) [8], Cu_3(InSnSbGaGe) [8], and (FeCoNiMn)$_3Sn_2$ [9] consisting of p-block elements have been also developed.

Several review papers have been published recently discussing different aspects of the formation and properties of HEICs. For example, Want et al. [10] briefly reviewed the fundamental rules for the formation of HEICs and their intricate functional properties. These HEICs are particularly interesting candidates for different catalytic reactions, including oxygen reduction [11, 12] and hydrogen evolution [13] reactions. Moreover, a TiZrHfCoNiCu HEIC was reported to exhibit superior yield strength of 1.58 GPa and fracture strength of 2.48 GPa [14]. Furthermore, it has been reported that microsegregation of the elements in HEICs during non-equilibrium solidification correlates with the existence of binary intermetallics with identical structure in the multicomponent HEIC phase [15]. It has been also revealed that mutual compensation of the fundamental properties of constituent atoms, electronegativity and atomic radius for example, are important factors determining the formation of single-phase HEICs [8]. However, the functional and mechanical properties of these HEICs are still unknown. Therefore, the major objective of this research is to study the magnetic properties of (CoCuFeMnNi)Al, (CoCuFeMnNi)Zn_3, Cu_3(InSnSbGaGe), (FeCoNiMn)$_3Sn_2$ and (FeCoMnNiCr)$_3Sn_2$ HEICs to provide more information about the effect of constituent elements and high entropy on their functional properties.

2. EXPERIMENTAL PROCEDURES

(CoCuFeMnNi)Al, (CoCuFeMnNi)Zn_3, Cu_3(InSnSbGaGe), (FeCoNiMn)$_3Sn_2$ and

[DOI: 10.22068/ijmse.3622]

$(FeCoMnNiCr)_3Sn_2$ were prepared by induction melting. Stoichiometric ratios of high purity (>99.9 wt.%) metal pieces were weighed and then transferred into alumina crucibles for melting. A blending of NaCl, CaF_2 and KCl was utilized as flux to protect the surface of the elements and prevent material losses. The melting was carried out under a reducing atmosphere (CO). For homogenization, the melts were given a 15-minute holding time. After this, the crucibles (cylindrical with an outer diameter of 20 mm and length of 15 mm) with melt were cooled in a laboratory atmosphere to reach the ambient temperature. The samples with a height of approximately 10 mm and a diameter of about 18 mm were harvested from the crucibles.

X-ray diffraction (XRD) analysis was undertaken by a Rigaku Ultima IV X-ray diffractometer using Cu–Kα radiation. Finely grounded powders were used for collecting XRD patterns. The sample's microstructure was studied via a scanning electron microscope (SEM) JEOL JSM7001F. The energy dispersive spectroscopy (EDS) detector (Oxford INCA X-max 80) on the SEM device was employed for analyzing the chemical composition of the samples.

The magnetization M of the samples as a function of the magnetic field was recorded at 5 K and 300 K in the magnetic field range from -20 kOe to 20 kOe. The changes in the magnetization of the samples were measured as a function of temperature M(T) from 5 K to 300 K under zero-field cooled (ZFC) and field-cooled (FC) regimes at a field of 10 kOe. All the measurements were performed on a Cryogenic CFS-9T-CVTI vibrating sample magnetometer.

3. RESULTS AND DISCUSSION

3.1. Microstructural Properties

Fig. 1 shows the SEM micrographs (in the back-scattered electron mode, BSE-SEM) and the related EDS maps of the HEIC samples. In the EDS map of (CoCuFeMnNi)Al, Cu-Mn and Ni-Co segregated regions can be observed (Fig. 1a). For $(FeCoMnNiCr)_3Sn_2$, a clear Fe-Cr segregation is observed in the EDS map, meanwhile, other elements indicate a nearly homogenous distribution in the microstructure of the alloy (Fig. 1b). Moreover, when Cr is removed from $(FeCoMnNiCr)_3Sn_2$, the segregated region is disappeared and the resultant $(FeCoMnNi)_3Sn_2$ indicates a uniform distribution of the constituent elements (Fig. 1c). Furthermore, the microstructure of $(CoCuFeMnNi)Zn_3$ (Fig. 1d) and $Cu_3(InSnSbGaGe)$ (Fig. 1e) HEICs exhibited a homogenous dispersion of the constituent elements with no observable segregation.

The XRD patterns, presented in Fig. 2, indicate that relatively pure ordered phases were obtained for all the samples. The XRD pattern of $(FeCoNiMn)_3Sn_2$ indicates that a nearly single hexagonal structure (Co_3Sn_2 prototype, space group P63/mmc, COD database code: 1524365) has been crystallized upon cooling from high temperatures. For $(FeCoMnNiCr)_3Sn_2$, the existence of FeCr (COD database code: 9016031) and $MnSn_2$-type (COD database code: 2207460) phases is observed from the obtained diffraction pattern. (CoCuFeMnNi)Al exhibits a single B2-type lattice (FeAl prototype with a space group $pm\bar{3}m$, COD database code: 1541193). Finally, crystal structures of $Cu_3(InSnSbGaGe)$ and $(CoCuFeMnNi)Zn_3$ can be adapted with a single hexagonal $Cu_{10}Sn_3$ (space group P63/m, COD database code: 1524806) and cubic γ-brass (space group $I\bar{4}3m$, COD database code: 4001929) prototype structures.

Table 1 shows the obtained chemical compositions of the samples from EDS analysis. It can be observed that all samples display a nearly similar chemical composition to those of their corresponding stoichiometric ratios and the constituent elements are highly integrated into the HEICs.

3.2. Magnetic Properties

To study the magnetic properties of the HEICs, magnetic hysteresis as well as field-cooled (FC) and zero-field cooled (ZFC) magnetizations as a function of temperature were recorded. The magnetic hysteresis loops of the samples are shown in Fig. 3. The hysteresis loop of (CoCuFeMnNi)Al indicates ferromagnetic behavior at 5 K (Fig. 3a), with a saturation magnetization of about Ms= 6.5 emu/g and a coercivity of about H_c= 100 Oe. It indicates a linear relationship between magnetization and magnetic field at 300 K, which is a feature of a paramagnetic or antiferromagnetic state. As shown in Fig. 3c, $(CoCuFeMnNi)Zn_3$ also indicates ferromagnetic behavior at 5 K, however, magnetization does not reach saturation level under an applied field of 2 T.

[DOI: 10.22068/ijmse.3622]

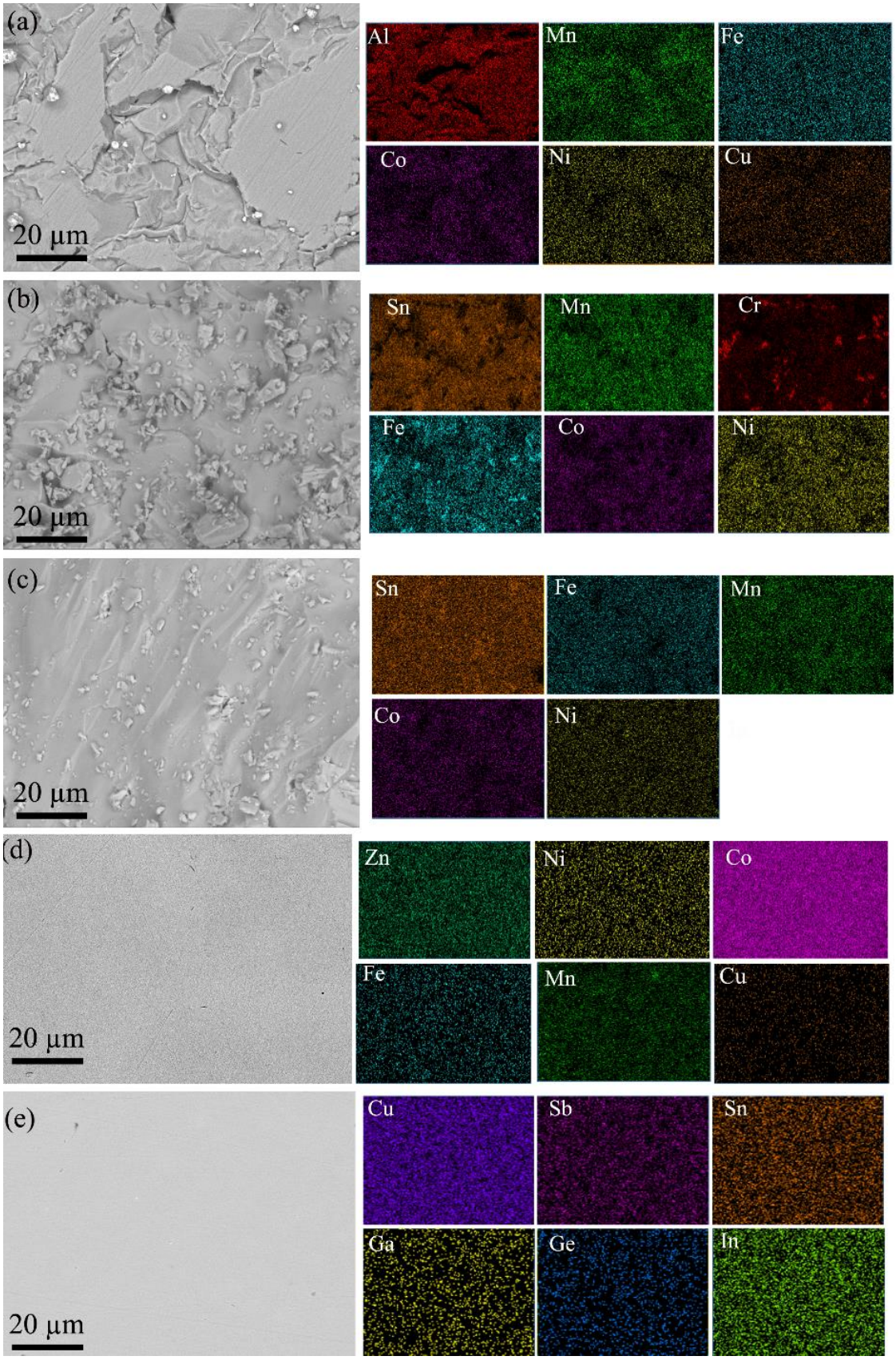

Fig. 1. BSE-SEM micrographs and the related maps of the (a) (CoCuFeMnNi)Al, (b) $(FeCoMnNiCr)_3Sn_2$, (c) $(FeCoMnNi)_3Sn_2$, (d) $(CoCuFeMnNi)Zn_3$ and (e) $Cu_3(InSnSbGaGe)$ HEICs in the as-cast state.

[DOI: 10.22068/ijmse.3622]

Table 1. Crystal structures and the corresponding chemical composition of the HEICs.

HEICs		Chemical Composition determined by EDS (at.%) Co	Cu	Fe	Mn	Ni	Cr	Al	Zn	Sn	Crystal structure
(CoCuFeMnNi)Al	Formula	10	10	10	10	10	-	50	-	-	B2 FeAl-type, COD: 1541193
	Average	10.17	9.83	9.77	9.96	9.44	-	50.83	-	-	
(CoCuFeMnNi)Zn_3	Formula	5	5	5	5	5	-	-	75	-	$D8_2$ cubic γ-brass, COD: 4001929
	Average	4.56	5.76	5.13	3.45	5.95	-	-	75.15	-	
(FeCoMnNiCr)$_3Sn_2$	Formula	12	-	12	12	12	12	-	-	40	Co_3Sn_2-type (COD: 1524365)+ CrFe (COD: 9016031)+ $MnSn_2$ (COD: 2207460)
	Average	12.68		11.65	12.5	11.54	11.74	-	-	39.89	
(FeCoNiMn)$_3Sn_2$	Formula	15		15	15	15	-	-	-	40	Co_3Sn_2-type (COD: 1524365)
	Average	15.76	-	14.98	14.49	14.64	-	-	-	40.13	
Cu_3(InSnSbGaGe)	Formula	75	5	5	5	5	5	-			$Cu_{10}Sn_3$-type (COD: 1524806)
	Average	75.24	5.13	5.11	5.26	4.42	4.85	-			

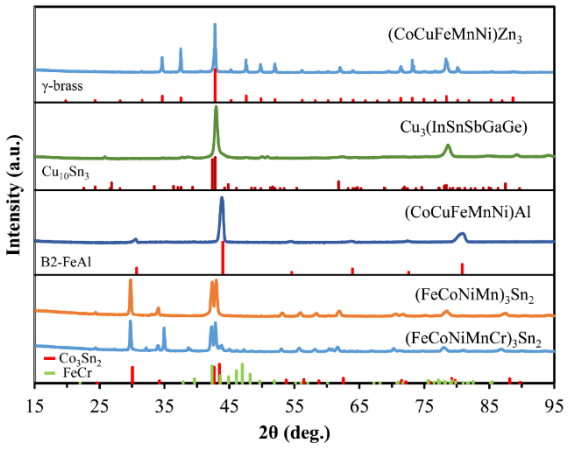

Fig. 2. XRD patterns of the HEICs in the as-cast state. The XRD patterns of the related reference phases are also shown.

This sample also indicates a linear dependence of magnetization vs. magnetic field at 300 K, i.e. paramagnetic or antiferromagnetic behavior. Moreover, (CoCuFeMnNi)Zn_3 exhibits a high coercivity of H_c= 1000 Oe, which is 10 times higher than that of (CoCuFeMnNi)Al. Magnetizations decrease with increasing temperature from 5 K to 300 K for both (CoCuFeMnNi)Al and (CoCuFeMnNi)Zn_3 HEICs. Under a magnetic field of 1 T, the magnetization of (CoCuFeMnNi)Zn_3 decreases from 1.13 emu/g at 5 K to 0.12 emu/g at 300 K, indicating a decline of about one order of magnitude. These values were 5 emu/g at 5 K and 0.15 emu/g at 300 K for (CoCuFeMnNi)Al. For both samples, the FC and ZFC highly coincide with each other and display a continuous decline in magnetization in the entire temperature range measured (Figs. 3b and d). The ZFC and FC curves did not display the occurrence of bifurcation, which typically occurs when magnetically inhomogeneous states are present in the materials. Moreover, the presence of different ordered magnetic phases (for example antiferromagnetic and ferromagnetic) in multi-phase materials could also lead to the bifurcation of ZFC and FC data. However, both (CoCuFeMnNi)Al and (CoCuFeMnNi)Zn_3 HEICs exhibited a uniform microstructure, in which the constituent elements were homogeneously distributed. This can be the reason for the absence of bifurcation in ZFC and FC data.

The magnetization curves of the other three (FeCoMnNiCr)$_3Sn_2$, (FeCoNiMn)$_3Sn_2$ and Cu_3(InSnSbGaGe) HEICs exhibited nearly linear changes with increasing magnetic field (Figs. 3e-g).

[DOI: 10.22068/ijmse.3622]

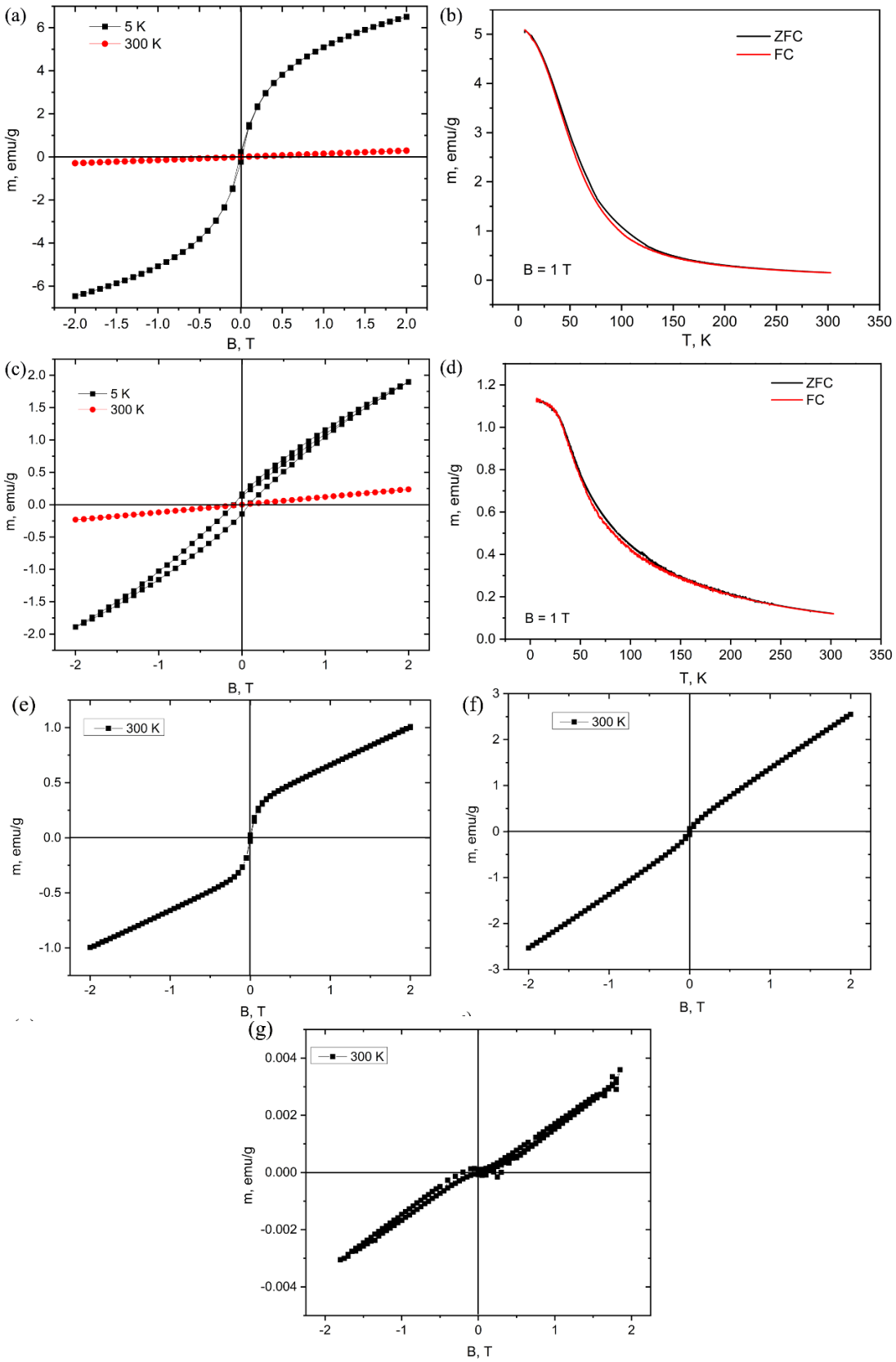

Fig. 3. Magnetization curves (a, c) and temperature dependence (b, d) of the field cooled (FC) and zero field cooled (ZFC) at 0.1 T for as-cast (CoCuFeMnNi)Al (a, b) and (CoCuFeMnNi)Zn_3 (c, d) HEICs. Magnetization curves for the as-cast $(FeCoMnNiCr)_3Sn_2$ (e), $(FeCoNiMn)_3Sn_2$ (f) and Cu_3(InSnSbGaGe) (g) HEICs at 300 K.

[DOI: 10.22068/ijmse.3622]

Ferrimagnetic or canted antiferromagnetic state indicates some extent of magnetization saturation and an aberration from the linear relationship between magnetization and magnetic field. It can be seen that magnetization of $(FeCoMnNiCr)_3Sn_2$ (Fig. 3e) indicates a higher aberration from a genuine linear relationship compared to the $(FeCoNiMn)_3Sn_2$ (Fig. 3f) and $Cu_3(InSnSbGaGe)$ (Fig. 3g) HEICs. This is probably due to the presence of FeCr and MnSn2-type second phases in $(FeCoMnNiCr)_3Sn_2$. As observed above, when Cr is removed from $(FeCoMnNiCr)_3Sn_2$, the resultant $(FeCoNiMn)_3Sn_2$ exhibits a single hexagonal Co_3Sn_2-type structure, which seems to behave like a ferrimagnetic or canted antiferromagnetic state with lower deviation from the linear behavior. However, it should be noted that $(FeCoNiMn)_3Sn_2$ displays higher magnetization (2.5 emu/g at B= 2T) compared to $(FeCoMnNiCr)_3Sn_2$ (1 emu/g at B= 2T) and the negligible magnetization of $Cu_3(InSnSbGaGe)$ (~0.004 emu/g).

3.3. The Correlation Between Microstructure/ Chemical Composition and Magnetic Properties

While saturation magnetization is mainly determined by chemical composition, coercivity is also affected by microstructural features such as lattice defects, grain size, elemental segregation, amount of magnetic/nonmagnetic phases, etc. [16, 17]. Here, all the samples were fabricated by the same induction melting process, and hence, the grain size, pores and internal stress may be considered relatively identical for all the samples. Therefore, the chemical composition, chemical inhomogeneity and the synergistic effect of local magnetic momentum of atoms occupying the high entropy sublattice are the main factors dictating the magnetic properties of HEICs. In this study, (CoCuFeMnNi)Al exhibited high saturation magnetization at 5 K consistent with the parallel and relatively high magnetic moments of Fe, Co and Ni. On the other hand, when Co-Cu-Fe-Mn-Ni are used to construct a high entropy sublattice with XZn_3 formula, the resultant $(CoCuFeMnNi)Zn_3$ displays lower magnetization and significantly higher coercivity at 5 K compared to (CoCuFeMnNi)Al owing to the diamagnetic nature of Zn that can strongly affect the ferromagnetic ordering of Fe, Mn, Co, and Ni atoms. The same reason may explain the linear magnetization and the ensuing ferrimagnetic or canted antiferromagnetic states in $(FeCoMnNiCr)_3Sn_2$ and $FeCoNiMn)_3Sn_2$ high entropy stannide at 300 K, considering the paramagnetic nature of Sn. Finally, $Cu_3(InSnSbGaGe)$ exhibited the lowest magnetization among all the investigated HEICs, which is consistent with the non-magnetic nature of the constituent elements. All these indicate the wide chemical composition window available in HEICs to tailor their chemistry and consequently magnetic or other functional properties.

4. CONCLUSIONS

In summary, the microstructure and magnetic properties of several HEICs with different types of orders were studied. (CoCuFeMnNi)Al and $(CoCuFeMnNi)Zn_3$ exhibited ferromagnetic behavior at 5 K and a linear relationship between magnetization and magnetic field at 300 K, which is a feature of a paramagnetic or antiferromagnetic state. $(FeCoMnNiCr)_3Sn_2$, $(FeCoNiMn)_3Sn_2$ and $Cu_3(InSnSbGaGe)$ HEICs also displayed an approximately linear dependence of magnetization at 300 K, with $(FeCoMnNiCr)_3Sn_2$ showing the highest deviation from pure linear dependency compared to $(FeCoNiMn)_3Sn_2$ and $Cu_3(InSnSbGaGe)$ HEICs. This can be attributed to the precipitation of FeCr and MnSn2-type second phases in $(FeCoMnNiCr)_3Sn_2$. As the fabricating process and consequently the grain size, pores and internal stress are almost identical for all the samples, chemical inhomogeneity and the synergistic effect of local magnetic momentum of atoms occupying the high entropy sublattice are the main factors dictating magnetic properties of HEICs. Finally, the magnetic properties of the samples could be further explained by the non-magnetic nature (diamagnetic or paramagnetic) of the constituent elements filling the low-entropy sublattices in the crystal structure of HEICs.

ACKNOWLEDGEMENT

The work was supported by the Russian Science Foundation, project No. 22-23-00243, https://rscf.ru/project/22-23-00243/.
Experimental studies of magnetic properties were performed using scientific instruments included in the Collective Equipment Centers “Ural-M”.

[DOI: 10.22068/ijmse.3622]

REFERENCES

[1]. Yao, K., Liu, L., Ren, J., Guo, Y., Liu, Y., Cao, Y., Feng, R., Wu, F., Qi, J., and Luo, J., "High-entropy intermetallic compound with ultra-high strength and thermal stability." Scripta Mater., 2021, 194, 113674.

[2]. Yang, T., Cao, B. X., Zhang, T. L., Zhao, Y., Liu, W. H., Kong, H. J., Luan, J. H., Kai, J. J., Kuo, W., and Liu, C. T., "Chemically complex intermetallic alloys: A new frontier for innovative structural materials." Mater. Today, 2022, 52, 161-174.

[3]. Yin, L., Guo, Y., and Guo, X., "Cocktail effect on RT5-type (R= rare earth, T= 3d transition metal) high entropy intermetallic compounds." J. Magn. Magn. Mater., 2022, 563, 169883.

[4]. Chen, W., Luo, S., Sun, M., Wu, X., Zhou, Y., Liao, Y., Tang, M., Fan, X., Huang, B., and Quan, Z., "High-entropy intermetallic PtRhBiSnSb nanoplates for highly efficient alcohol oxidation electrocatalysis." Adv. Mater., 2022, 34, 2206276.

[5]. Ostovari Moghaddam, A., Abdollahzadeh, A., Samodurova, M., Shaburova, N., Mikhailov, D., Fereidonnejad, R., Zhivulin, V., and Trofimov, E., "Novel high entropy intermetallic compounds: Synthesis and detonation spraying." Intermetallics, 2022, 146, 107591.

[6]. Uporov, S. A., Ryltsev, R. E., Estemirova, S. K., Sterkhov, E. V., and Chtchelkatchev, N. M., "Stable high-entropy TiZrHfNbVCrMoMnFeCoNiAl Laves phase." Scripta Mater., 2021, 193, 108-111.

[7]. Wang, D., Chen, Z., Wu, Y., Huang, Y. C., Tao, L., Chen, J., Dong, C. L., Singh, C. V., and Wang, S., "Structurally ordered high-entropy intermetallic nanoparticles with enhanced C–C bond cleavage for ethanol oxidation." SmartMat, 2022, 4, e1117.

[8]. Trofimov, E., Moghaddam, A. O., Zaitseva, O., Fereidonnejad, R., Naseri, M., Shaburova, N., and Mikhailov, D., "Synthesis and characterization of intermetallic compounds with one medium-or high-entropy sublattice occupied by p-block elements." Mater. Chem. Phys., 2023, 301, 127596.

[9]. Trofimov, E., Ostovari Moghaddam, A., Zaitseva, O., Fereidonnejad, R., and Mikhailov, D., "Unraveling new single phase high entropy stannide by experimental screening of the as-cast samples." Mater. Lett., 2023, 335, 133861.

[10]. Wang, H., He, Q.-F., and Yang, Y., "High-entropy intermetallics: from alloy design to structural and functional properties." Rare Metals, 2022, 41, 1989-2001.

[11]. Chen, T., Qiu, C., Zhang, X., Wang, H., Song, J., Zhang, K., Yang, T., Zuo, Y., Yang, Y., and Gao, C., "An Ultrasmall Ordered High-Entropy Intermetallic with Multiple Active Sites for the Oxygen Reduction Reaction." J. Am. Chem. Soc., 2023, 146, 1174-1184.

[12]. Wang, Y., Zhang, X. Y., He, H., Chen, J. J., and Liu, B., "Ordered Mesoporous High-Entropy Intermetallics for Efficient Oxygen Reduction Electrocatalysis." Adv. Energy Mater., 2024, 14, 2303923.

[13]. Wang, Y., Gong, N., Liu, H., Ma, W., Hippalgaonkar, K., Liu, Z., and Huang, Y., "Ordering-Dependent Hydrogen Evolution and Oxygen Reduction Electrocatalysis of High-Entropy Intermetallic $Pt_4FeCoCuNi$." Adv. Mater., 2023, 35, 2302067.

[14]. Duan, K., Liu, L., Yao, K., Zhang, X., Liu, B., Qi, J., Chen, M., Zhao, R., and Wu, F., "High-entropy intermetallics with striking high strength and thermal stability." Mater. Lett., 2022, 321, 132424.

[15]. Trofimov, E., Ostovari Moghaddam, A., Litvinyuk, K., and Mikhailov, D., "Microsegregation in high-entropy intermetallic compounds." J. Alloys Compd., 2023, 934, 168021.

[16]. Dehghaniyan, S. F. and Sharafi, S., "Synthesis and Characterization of Nanostructured (Fe80 Ni20)1-x Crx (x= 0, 4) Alloys Using Mechanical Alloying and Density Functional Theory." IJMSE, 2024, 21, 1-12.

Bandekar, A., Tirmali, P., Gaikar, P., Kulkarni, S., and Pradhan, N., "Sol-gel Approach for the Synthesis and Characterization of Mg and Cu Substituted Mn-Zn Ferrite Nanoparticles." IJMSE, 2024, 21, 42-50.

[DOI: 10.22068/ijmse.3622]